

Gamma-ray shielding study of light to heavyweight concretes using MCNP-4C code

Reza Bagheri¹ · Alireza Khorrami Moghaddam² · Ali Yousefi¹

Received: 5 July 2015 / Revised: 15 August 2016 / Accepted: 29 August 2016 / Published online: 24 December 2016
© Shanghai Institute of Applied Physics, Chinese Academy of Sciences, Chinese Nuclear Society, Science Press China and Springer Science+Business Media Singapore 2016

Abstract In this work, linear and mass attenuation coefficients, half and tenth-value layers, effective atomic number and electron density of different types of concretes were determined at 316.51, 468.07, 511, 662, 1173 and 1332 keV using MCNP-4C code and WinXCom programs. The MCNP-4C and WinXCom results agreed well with each other, with differences of $<\pm 1.9\%$. The results agreed with available experimental data, too, with differences of $<\pm 6\%$. The MCNP-4C results showed better agreement with the experimental data than the WinXCom results. Also, it was found that the effective electron density of studied concretes varies in the range of $(2.83\text{--}3.2) \times 10^{23}$ electron/g.

Keywords Concrete · Shielding · MCNP-4C · WinXCom · Mass attenuation coefficient · Effective atomic number and electron density

1 Introduction

Today, utilization of gamma-ray sources with care and safety is essential [1–3]. Concrete, a common construction material, is widely used against ionizing radiations [4–7]. For this purpose, various types of heavy density concretes have been developed, consisting of heavy elements such as

iron, barium and titanium in their structure [8–12]. Extensive studies on radiation shielding characteristics of various concretes and aggregates were published by Bashter [6, 9], Bashter et al. [7, 8]. They calculated the linear and mass attenuation coefficients of seven types of concretes at photon energies from 10 keV to 1 GeV [6]. Akkurt et al. [2] used ^{137}Cs and ^{60}Co gamma-ray sources to measure photon attenuation coefficients of barite and concrete produced with barite in different rates. Han et al. [5] determined mass attenuation coefficients, effective atomic and electron numbers for some natural minerals usable in concretes. Stankovic et al. [10] calculated the transmission factor and the mass attenuation coefficients in ordinary and barite concretes for 511 and 662 keV photons by the FOTELP-2K6 Monte Carlo code. The shielding of gamma rays and fast neutrons was studied for concretes containing different lime/silica ratios using WinXCom and MERCSEF-N program by El-Khayatt [11]. Using the Monte Carlo code of MCNP-4B, Singh et al. [12] simulated the linear and mass attenuation coefficients of photons at 1.5–6 MeV and the tenth-value layer thickness of seven types of concretes used in nuclear reactor technology, and by comparing the simulation results with experimental data and XCOM photon cross-sectional database, they showed that simulation produced reliable shielding data for this use of concretes.

In this research, eight types of concretes including ordinary (O), hematite–serpentine (HS), serpentine (S), ilmenite–limonite (IL), basalt–magnetite (BM), barite (B), steel–scrap (SS) and steel–magnetite (SM) were considered as shielding against gamma rays. The linear and mass attenuation coefficients (μ and μ_m), effective atomic number and electron density (Z_{eff} and N_{eff}), total atomic and electronic cross sections (σ_a and σ_e), half-value layer (HVL) and tenth-value layer (TVL) were calculated on

✉ Reza Bagheri
reza_bagheri@aut.ac.ir

¹ Nuclear Fuel Cycle Research School (NFCRS), Nuclear Science and Technology Research Institute (NSTRI), Tehran 14155-1339, Iran

² Radiology Department, Paramedical Faculty, Mazandaran University of Medical Sciences, Sari, Mazandaran 14536-33143, Iran

basis of elemental compositions of the concretes using MCNP-4C Monte Carlo code and WinXCom program. Percentage composition of mentioned concretes and their densities are given in Table 1 [2, 6–9].

Gamma-ray sources of ^{192}Ir (316.51 keV, 82.81%; 468.07 keV, 47.83%), ^{60}Co (1173 keV, 100%; 1332 keV, 100%) and ^{137}Cs (662 keV, 94.6%), together with 511 keV gamma ray of positron annihilation, were used in the simulation [10, 13–16].

On the other hand, the theoretical values of mass attenuation coefficients for different elements, compounds and mixtures over wide range of photon energy have been tabulated by Hubbell and Seltzer [17]. Using such tables, mass attenuation coefficients at energies of 1 keV to 100 GeV [18, 19] can be calculated by the WinXCom program. So, we used it to determine shielding characteristics of the concretes and compared them with MCNP results. Also, our results were compared with available experimental data [2, 6, 20].

2 Materials and methods

2.1 Geometry of concretes

Cylindrical geometries were employed for modeling of concrete samples. Eight sections of sub-cylinders of $\Phi 30\text{ cm} \times 5\text{ cm}$ were considered for every type of concretes and set on Z axis in tandem. Figure 1 shows the simulated geometry.

2.2 Source specification

Sources were considered as planar, collimated and monoenergetic with uniform distribution of radioactive

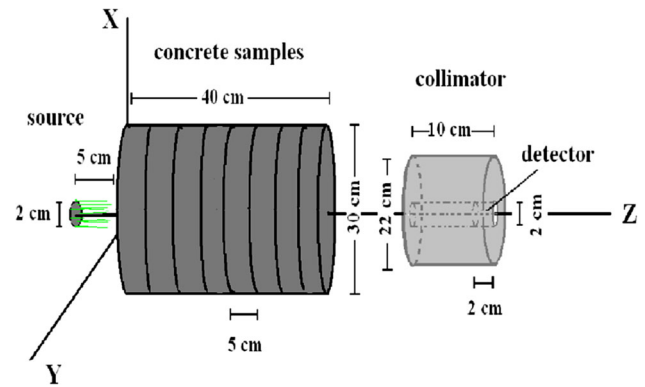


Fig. 1 Geometry of modeled configuration (sizes are not in scale)

material that emits gamma-ray beams perpendicular to front face of the samples (in direction of Z axis). A disk source of $\Phi 2\text{ cm}$, parallel to the X–Y plane and origin on Z axis, was defined in data card of the MCNP code with ERG, PAR, POS and DIR commands for energy and type of particle, position and direction of source, respectively.

2.3 Materials specification of concretes

Elemental composition of concrete depends mainly on the mix proportions and chemical composition of the materials. The percentages by weight of the elements in the concretes are presented in Table 2 [6, 10].

2.4 Detector geometry and tally definition

A small cylinder of $\Phi 2\text{ cm} \times 2\text{ cm}$ was considered as detector volume and set inside the collimator at 58 cm

Table 1 Percentage composition of concretes and their densities

Concrete types	Ordinary	Hematite–serpentine	Serpentine	Ilmenite–limonite	Basalt–magnetite	Barite	Steel–scrap	Steel–magnetite
Portland cement	11.82	13.19	15.94	12.44	12.42	10.77	8.81	7.55
Sand	26.71	–	27.35	–	–	–	26.08	–
Gravel	54.96	–	–	–	–	–	–	–
Ilmenite	–	–	–	68.5	–	–	–	–
Limonite	–	–	–	14.75	–	–	–	–
Hematite	–	56.88	–	–	–	–	–	–
Barite	–	–	–	–	–	83.75	–	–
Basalt	–	–	–	–	38.51	–	–	–
Serpentine	–	21.03	48.33	–	–	–	–	–
Magnetite	–	–	–	–	41.62	–	–	26.19
Steel–scrap	–	–	–	–	–	–	60.70	61.73
Water	6.51	8.90	8.38	4.30	7.45	5.48	4.41	4.53
Density(g cm^{-3})	2.3	2.5	2.6	2.9	3.05	3.35	4	5.1

Table 2 Atomic compositions (in wt %) of the concrete types

Elements	O	HS	S	IL	BM	B	SS	SM
¹ H	0.94	1.29	7.20	0.66	0.83	0.36	0.7	0.51
⁶ C	0.09	–	0.15	–	–	–	0.09	–
⁸ O	53.66	43.51	55.6	36.45	42.3	31.16	21.09	15.7
¹¹ Na	0.46	–	–	–	1.06	–	0.45	–
¹² Mg	0.12	6.64	10.20	0.15	2.2	0.12	0.09	0.58
¹³ Al	1.32	1.67	2.50	0.8	4.22	0.42	1.2	0.66
¹⁴ Si	36.74	10.53	17.55	3.06	13.2	1.05	10.49	2.68
¹⁵ P	–	–	–	–	0.2	–	–	0.08
¹⁶ S	0.08	0.09	–	0.08	0.09	10.78	0.06	0.06
¹⁹ K	0.31	–	0.08	–	0.29	–	0.3	–
²⁰ Ca	5.65	5.97	5.64	5.83	8.88	5.02	4.28	3.95
²² Ti	–	–	–	16.04	0.6	–	–	–
²⁵ Mm	–	–	–	–	0.12	–	–	0.07
²⁶ Fe	0.63	30.30	1.08	36.93	26.01	4.75	61.25	75.71
⁵⁶ Ba	–	–	–	–	–	46.34	–	–

from the source. A $\Phi 22$ cm \times 10 cm lead cylinder with a $\Phi 2$ cm \times 10 cm hole was used as the collimator (Fig. 1).

Tally F4 was used to obtain MCNP-4C simulated data. This tally calculates average flux in a cell (detector volume) for only one incident gamma photon.

The simulations were performed with 1–10 million histories depending on type and thickness of concrete specimens. All simulated results were reported with <0.1% error.

3 Results and discussion

3.1 Transmission factor

The transmission factors of a concrete type can be defined by Eq. (1)

$$T(E, d) = \Phi(E, d) / \Phi(E, 0), \quad (1)$$

where E is the gamma-ray energy (keV), d is thickness (cm) of shielding concrete, $\Phi(E, d)$ is the flux in the detector attained by the Tally F4 and $\Phi(E, 0)$ is the flux in absence of any shielding material. The transmission factors for selected gamma rays as a function of concrete thickness are shown in Fig. 2.

Of all the concrete types, the ordinary concrete with the least density has the least amount of attenuation (the most amount of transmission), while the steel-magnetite concrete with the greatest density has the greatest amount of attenuation (the least amount of transmission), even though the barite and ilmenite–limonite concretes contain high atomic number elements (Ba, Ti). Also, the transmission factors of concretes span from 1 to $<10^{-9}$.

3.2 Linear and mass attenuation coefficients, HVL and TVL values of concretes

Linear and mass attenuation coefficients of the concretes (μ and μ_m) were derived from transmission factor curves through fitting Lambert law ($I = I_0 e^{-\mu x}$) using MATLAB version 7.10.0.499. The results are given in Table 3.

The mass attenuation coefficients of concretes were also calculated using WinXCom program data using Eq. (2)

$$\mu_m = \sum w_i \mu_{m,i}, \quad (i = 1 \rightarrow n), \quad (2)$$

where w_i and $\mu_{m,i}$ (obtained directly from WinXCom program) are percentage by weight and mass attenuation coefficient of i th element in the concrete, respectively. The linear attenuation coefficients were calculated by multiplying mass attenuation coefficient of each type of concrete by its density. The linear and mass attenuation coefficients of concretes obtained by WinXCom program for different photon energies are presented in Table 4.

It is completely clear from both tables that the MC-simulated data and WinXCom-calculated data are very close to each other. The percentage differences between the MCNP and WinXCom results of mass attenuation coefficients for all gamma rays and concrete types range from -1.89 to 1.72% , averaged at 0.53% .

In Tables 3 and 4, at 316.51 keV, the linear attenuation coefficient of barite concrete (density = 3.35 g cm^{-3}) is greater than that of steel–scrap value (density = 4 g cm^{-3}), unlike the general tendency that the linear attenuation coefficient increases with the density. This discrepancy could be due to the photoelectric effect. This effect is favored by low-energy photons and high atomic number absorbers, so that cross section for this

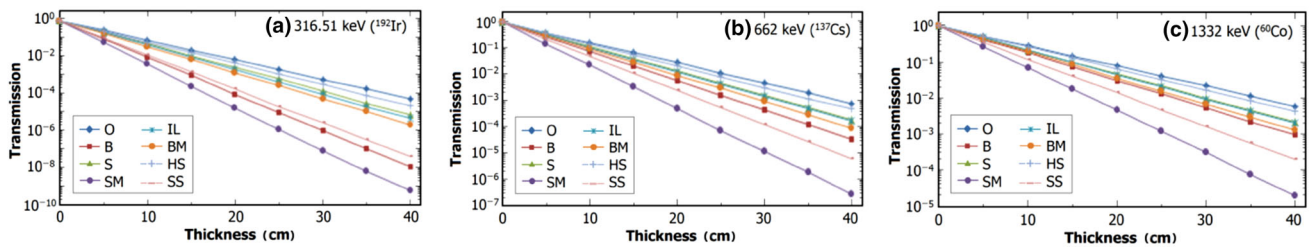


Fig. 2 Transmission factors of concretes to gamma rays of different energies

Table 3 MC-simulated linear (μ , cm^{-1}) and mass (μ_m , $\text{cm}^2 \text{g}^{-1}$) attenuation coefficients of the concretes for gamma rays

Concrete type	Density (g cm^{-3})	316.51 keV		468.07 keV		511 keV		662 keV		1173 keV		1332 keV	
		μ	μ_m	μ	μ_m	μ	μ_m	μ	μ_m	μ	μ_m	μ	μ_m
Ordinary	2.3	0.244	0.106	0.208	0.090	0.200	0.087	0.179	0.078	0.136	0.059	0.127	0.055
Hematite–serpentine	2.5	0.266	0.107	0.224	0.090	0.216	0.086	0.192	0.077	0.145	0.059	0.136	0.054
Serpentine	2.6	0.291	0.112	0.249	0.096	0.240	0.092	0.214	0.082	0.163	0.062	0.152	0.059
Ilmenite–limonite	2.9	0.306	0.105	0.255	0.088	0.246	0.085	0.218	0.075	0.165	0.057	0.154	0.053
Basalt–magnetite	3.05	0.323	0.106	0.272	0.089	0.262	0.086	0.233	0.076	0.176	0.058	0.165	0.054
Barite	3.35	0.456	0.136	0.324	0.097	0.305	0.091	0.258	0.077	0.186	0.055	0.173	0.052
Steel–scrap	4	0.426	0.106	0.353	0.088	0.340	0.085	0.300	0.075	0.227	0.057	0.212	0.053
Steel–magnetite	5.11	0.542	0.106	0.447	0.087	0.429	0.084	0.379	0.074	0.285	0.056	0.268	0.052

Table 4 Linear (cm^{-1}) and mass ($\text{cm}^2 \text{g}^{-1}$) attenuation coefficients of the concretes for studied gamma rays using WinXCom program

Concrete type	Density (g cm^{-3})	316.51 keV		468.07 keV		511 keV		662 keV		1173 keV		1332 keV	
		μ	μ_m	μ	μ_m	μ	μ_m	μ	μ_m	μ	μ_m	μ	μ_m
Ordinary	2.3	0.245	0.106	0.208	0.090	0.201	0.087	0.179	0.078	0.136	0.059	0.128	0.056
Hematite–serpentine	2.5	0.267	0.107	0.224	0.089	0.216	0.087	0.193	0.077	0.146	0.058	0.137	0.055
Serpentine	2.6	0.292	0.112	0.247	0.095	0.241	0.093	0.215	0.083	0.163	0.063	0.153	0.059
Ilmenite–limonite	2.9	0.307	0.106	0.256	0.088	0.247	0.086	0.219	0.076	0.166	0.057	0.155	0.054
Basalt–magnetite	3.05	0.324	0.106	0.269	0.088	0.263	0.086	0.234	0.077	0.177	0.058	0.166	0.054
Barite	3.35	0.461	0.138	0.327	0.098	0.307	0.092	0.260	0.078	0.187	0.056	0.175	0.052
Steel–scrap	4	0.427	0.107	0.353	0.088	0.340	0.086	0.302	0.075	0.228	0.057	0.214	0.053
Steel–magnetite	5.11	0.544	0.107	0.448	0.088	0.432	0.085	0.381	0.075	0.288	0.056	0.270	0.053

reaction varies approximately as $Z^n/E^{3.5}$, where the exponent n varies between 4 and 5 over the gamma-ray energy region of interest [21]. According to this fraction, at low energetic gamma rays, barite concrete with components of high atomic number elements (especially barium) has greater linear attenuation coefficient than those of the other concretes. This makes barite aggregate a good material for shielding against gamma rays.

Figure 3 shows the half-value layer ($\text{HVL} = \ln 2/\mu$) and tenth-value layer ($\text{TVL} = \ln 10/\mu$) of the concretes, i.e., the HVL and TVL quantities are defined as the concrete thickness which reduces photon intensity to half and tenth of its initial value, respectively.

Of course, the HVL and TVL values decrease with increasing density and increase with the incident photon energy, but at 316.51 keV the values of barite concrete are smaller than those of steel–scrap, due to the photoelectric effect of barite concrete, as mentioned above.

The calculated data were compared with available experimental results of some concretes [2, 6, 20] (Tables 5 and 6). Generally, the calculation results are in accordance with the experimental data. The percentage differences between calculated and experimental data of HVL and TVL range from -2.94 to 15.45% , being $<5\%$ for ordinary concrete at 662 keV and $<3\%$ for barite

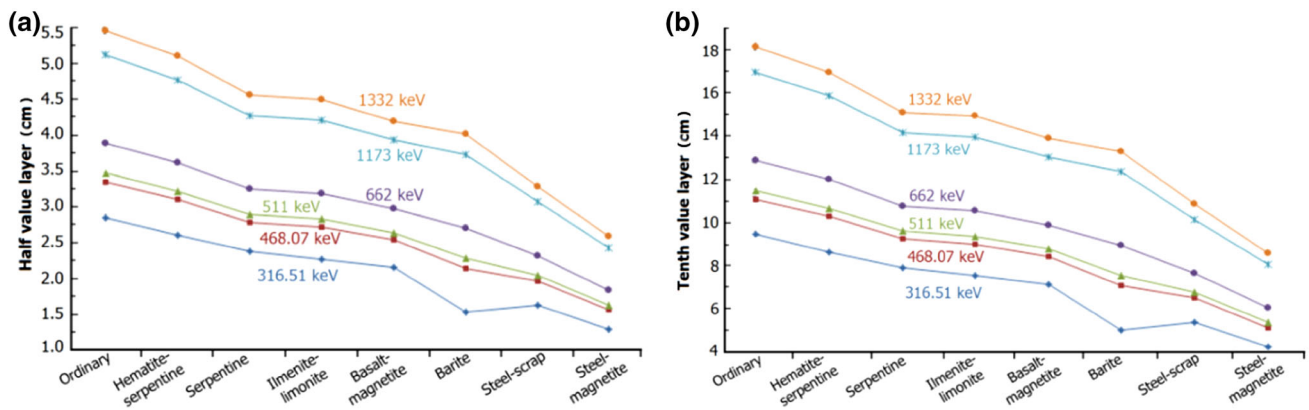


Fig. 3 Half-value layer (a) and tenth-value layer (b) of studied concretes for selected photon energies

Table 5 Measured and calculated results of HVL and TVL for ordinary and barite concretes at 662 keV gamma-ray energy

Concrete type	Ordinary		Barite	
	662	1332	662	1332
Gamma energy (keV)				
HVL (cm)				
Refs. [2, 20]	3.71	–	2.33	4.08
MCNP-4C (percentage difference)	3.88 (4.58%)	5.46	2.69 (15.45%)	4.00 (–2.00%)
WinXCom (percentage difference)	3.87 (4.31%)	5.42	2.67 (14.59%)	3.96 (–2.94%)
TVL (cm)				
Refs. [2, 20]	12.31	–	7.75	13.54
MCNP-4C (percentage difference)	12.89 (4.71%)	18.13	8.94 (15.35%)	13.30 (–1.77)
WinXCom (percentage difference)	12.86 (4.46%)	17.99	8.86 (14.32%)	13.16 (–2.81%)

Densities of the ordinary concrete samples in Refs. [2, 20] and this work are 2.46, 2.31 and 2.30 g cm⁻³, respectively, while they are 3.46, 3.45 and 3.35 g cm⁻³ for the barite concrete samples in Refs. [2, 20], respectively

Table 6 Experimental [6] and calculated results of linear attenuation coefficients (cm⁻¹) at 1.5 MeV

Concrete type	Ref. [6]	MCNP-4C (percentage difference)	WinXCom (percentage difference)
Ordinary	0.164	0.121 (–26.22%)	0.120 (–26.83%)
Hematite–serpentine	0.124	0.128 (3.23%)	0.129 (4.03%)
Ilmenite–limonite	0.159	0.146 (–8.18%)	0.146 (–8.18%)
Basalt–magnetite	0.139	0.156 (12.23%)	0.157 (12.95%)
Steel–scrap	0.196	0.201 (2.55%)	0.201 (2.55%)
Steel–magnetite	0.220	0.253 (15.00%)	0.254 (15.45%)

concrete at 1332 keV. The percentage differences between calculated and experimental data of linear attenuation coefficients at 1.5 MeV range from –26.83 to 15.45% (Table 6). Due to differences in the densities and elemental compositions among the concretes in this work and Refs. [2, 6, 20], some inequalities between experimental and calculated data were observed. Differences in geometry of simulation relative to experiment lead to little discrepancy in calculated and measured values. Reported error of experimental work in Table 6 is $\pm 10\%$ [6].

3.3 Effective atomic number and electron density of concretes

The total atomic cross sections for concretes are calculated from the simulated values of μ_m using Eq. (3) [22]:

$$\sigma_a = \mu_m N / N_A, \tag{3}$$

where N is the atomic mass of concrete and N_A is the Avogadro’s number. Also, the σ_a and the total electronic cross sections, σ_e , for WinXCom program can be calculated from Eqs. (4) and (5) [23]:

Table 7 MCNP-4C (MC) and WinXCom (WXC) values of effective atomic numbers (Z_{eff}) for studied concretes

Concrete types	Density (g cm ⁻³)	316.51 keV		468.07 keV		511 keV		662 keV		1173 keV		1332 keV	
		MC	WXC	MC	WXC	MC	WX	MC	WXC	MC	WXC	MC	WXC
Ordinary	2.3	8.62	8.66	8.64	8.62	8.63	8.61	8.60	8.63	8.58	8.63	8.57	8.64
Hematite–serpentine	2.5	9.31	9.34	9.24	9.22	9.25	9.16	9.17	9.20	9.12	9.18	9.11	9.18
Serpentine	2.6	4.48	4.50	4.49	4.46	4.47	4.47	4.47	4.48	4.45	4.48	4.45	4.48
Ilmenite–limonite	2.9	11.68	11.73	11.56	11.57	11.56	11.50	11.47	11.52	11.42	11.48	11.41	11.49
Basalt–magnetite	3.05	10.09	10.14	10.13	10.01	10.07	9.96	9.97	10.01	9.93	9.98	9.93	9.99
Barite	3.35	17.99	18.18	15.85	15.98	15.92	14.88	14.95	15.08	14.39	14.49	14.30	14.46
Steel–scrap	4	13.43	13.47	13.28	13.27	13.35	13.13	13.12	13.20	13.06	13.15	13.05	13.15
Steel–magnetite	5.11	15.73	15.83	15.53	15.60	15.69	15.43	15.40	15.51	15.30	15.45	15.31	15.45

Table 8 MCNP-4C and WinXCom values of effective electron density ($N_{\text{eff}} \times 10^{23}$ electron/g) for studied concretes

Concrete type	316.51 keV		468.07 keV		511 keV		662 keV		1173 keV		1332 keV	
	MC	WXC	MC	WXC	MC	WXC	MC	WXC	MC	WXC	MC	WXC
Ordinary	3.03	3.04	3.04	3.03	3.04	3.03	3.02	3.03	3.02	3.03	3.01	3.03
Hematite–serpentine	3.03	3.04	3.01	3.00	3.01	3.00	2.98	2.99	2.97	2.99	2.97	2.99
Serpentine	3.22	3.23	3.22	3.20	3.22	3.20	3.21	3.22	3.20	3.22	3.20	3.22
Ilmenite–limonite	2.97	2.98	2.94	2.94	2.94	2.94	2.92	2.93	2.90	2.92	2.90	2.92
Basalt–magnetite	3.01	3.02	3.02	2.98	3.02	2.98	2.97	2.98	2.96	2.98	2.96	2.98
Barite	3.52	3.55	3.10	3.12	3.10	3.12	2.92	2.95	2.81	2.83	2.80	2.83
Steel–scrap	2.97	2.98	2.94	2.94	2.94	2.94	2.90	2.92	2.89	2.91	2.89	2.91
Steel–magnetite	2.93	2.95	2.89	2.90	2.89	2.90	2.87	2.89	2.85	2.88	2.85	2.88

$$\sigma_a = \left(\sum f_i N_i \mu_{m,i} \right) / N_A, \quad (i = 1 \rightarrow n), \quad (4)$$

$$\sigma_e = \left(\sum f_i N_i \mu_{m,i} / Z_i \right) / N_A, \quad (i = 1 \rightarrow n), \quad (5)$$

where f_i denotes the fractional abundance of the i th element with respect to the number of atoms such that $f_1 + f_2 + f_3 + \dots + f_i = 1$, and Z_i and N_i are the atomic number and atomic mass of the i th element, respectively. Finally, effective atomic number (Z_{eff}) and effective electron density (N_{eff}) of the concretes are calculated by Eqs. (6) and (7) [3] (Tables 7 and 8):

$$Z_{\text{eff}} = \sigma_a / \sigma_e, \quad (6)$$

$$N_{\text{eff}} = \mu_m / \sigma_e. \quad (7)$$

Both tables show good agreement between MCNP-4C code and WinXCom program results. In Table 7, the Z_{eff} value approximately increases with the concrete density and decreases with increasing photon energy. This is due to high atomic number elements ratio in material (especially barium in barite concrete), and concretes of high Z_{eff} values will effectively absorb incoming photons. Of all the concretes, the effective atomic number of steel-magnetite is the greatest, while that of serpentine concretes is the lowest. Iron ($Z = 26$) and oxygen ($Z = 8$) as heavy and light

weight elements constitute the greatest elemental portion in these concretes (about 76 and 56%, respectively). In Table 8, the effective electron density of studied concretes varies from 2.83×10^{23} to 3.2×10^{23} electron/g. It decreases slowly with increasing photon energy, and serpentine and barite concretes have the greatest and the lowest values of effective electron densities, respectively.

4 Conclusion

Transmission factors, linear and mass attenuation coefficients, HVL and TVL values, effective atomic numbers and electron densities for ordinary, hematite–serpentine, serpentine, ilmenite–limonite, basalt–magnetite, barite, steel–scrap and steel–magnetite concretes at 316.51, 468.07, 511, 662, 1173 and 1332 keV gamma ray energies were simulated and calculated using MCNP-4C Code and WinXCom program and were compared with available experimental data. It was found that results by MCNP code and WinXCom program were in good agreement with each other. Effective electron density of studied concretes was about 3×10^{23} electron/g, and steel-magnetite and barite concretes have got the greatest value of effective atomic

number. This work indicates that simulation using the MCNP-4C code provides reliable values of linear attenuation coefficients for various concretes within $\pm 6\%$ in comparison with experimental values.

References

- V.P. Singh, N.M. Badiger, Comprehensive study of energy absorption and exposure buildup factor for concrete shielding in photon energy range 0.015–15 MeV up to 40 mfp penetration depth: dependency of density, chemical element, photon energy. *Nucl. Energy Sci. Technol.* **7**, 75–99 (2012). doi:[10.1504/IJN-EST.2012.046987](https://doi.org/10.1504/IJN-EST.2012.046987)
- I. Akkurt, H. Akyildirim, B. Mavi et al., Photon attenuation coefficients of concrete include barite in different rate. *Ann. Nucl. Energy* **37**, 910–914 (2010). doi:[10.1016/j.anucene.2010.04.001](https://doi.org/10.1016/j.anucene.2010.04.001)
- C. Boottjomchai, J. Laopaiboon, C. Yenchai et al., Gamma-ray shielding and structural properties of barium–bismuth–borosilicate glasses. *Radiat. Phys. Chem.* **81**, 785–790 (2012). doi:[10.1016/j.radphyschem.2012.01.049](https://doi.org/10.1016/j.radphyschem.2012.01.049)
- V.P. Singh, M.E. Medhat, S.P. Shirmardi, Comparative studies on shielding properties of some steel alloys using Geant4, MCNP, WinXCOM and experimental results. *Radiat. Phys. Chem.* **106**, 255–260 (2015). doi:[10.1016/j.radphyschem.2014.07.002](https://doi.org/10.1016/j.radphyschem.2014.07.002)
- I. Han, L. Demir, M. Sahin, Determination of mass attenuation coefficients, effective atomic and electron numbers for some natural minerals. *Radiat. Phys. Chem.* **78**, 760–764 (2009). doi:[10.1016/j.radphyschem.2009.03.077](https://doi.org/10.1016/j.radphyschem.2009.03.077)
- I.I. Bashter, Calculation of radiation attenuation coefficients for shielding concretes. *Ann. Nucl. Energy* **24**, 1389–1401 (1997). doi:[10.1016/S0306-4549\(97\)00003-0](https://doi.org/10.1016/S0306-4549(97)00003-0)
- I.I. Bashter, A.S. Makarious, A.A. El-Sayed, Investigation of hematite–serpentine and ilmenite–limonite concretes for reactor radiation shielding. *Ann. Nucl. Energy* **23**, 65–71 (1996). doi:[10.1016/0306-4549\(95\)00011-G](https://doi.org/10.1016/0306-4549(95)00011-G)
- I.I. Bashter, A.A. El-Sayed, A.A. Samir, Magnetite ores with steel or basalt for concrete radiation shielding. *Jpn. J. Appl. Phys.* **36**, 3692–3696 (1997). doi:[10.1143/JJAP.36.3692](https://doi.org/10.1143/JJAP.36.3692)
- I.I. Bashter, Radiation attenuation and nuclear properties of high density concrete made with steel aggregates. *Radiat. Eff. Defects Solids* **140**, 351–364 (1997). doi:[10.1080/10420159708216859](https://doi.org/10.1080/10420159708216859)
- S.J. Stankovic, R.D. Ilic, K. Jankovic et al., Gamma radiation absorption characteristics of concrete with components of different type materials. *Acta Phys. Pol., A* **117**, 812–816 (2010). doi:[10.12693/APhysPolA.117.812](https://doi.org/10.12693/APhysPolA.117.812)
- A.M. El-Khayatt, Radiation shielding of concretes containing different lime/silica ratios. *Ann. Nucl. Energy* **37**, 991–995 (2010). doi:[10.1016/j.anucene.2010.03.001](https://doi.org/10.1016/j.anucene.2010.03.001)
- V.P. Singh, A.M. Ali, N.M. Badiger et al., Monte Carlo simulation of gamma ray shielding parameters of concretes. *Nucl. Eng. Des.* **265**, 1071–1077 (2013). doi:[10.1016/j.nucengdes.2013.10.008](https://doi.org/10.1016/j.nucengdes.2013.10.008)
- G. Pfennig, H. Klewe-Nebenius, W. Seelmann-Eggebert, *Karlsruher nkliidkarte*, 6th edn. (Longman Press, Harlow, 1995)
- S.P. Shirmardi, M. Shamsaei, M. Naserpour, Comparison of photon attenuation coefficients of various barite concretes and lead by MCNP code, XCOM and experimental data. *Ann. Nucl. Energy* **55**, 288–291 (2013). doi:[10.1016/j.anucene.2013.01.002](https://doi.org/10.1016/j.anucene.2013.01.002)
- Sh Sharifi, R. Bagheri, S.P. Shirmardi, Comparison of shielding properties for ordinary, barite, serpentine and steel–magnetite concretes using MCNP-4C code and available experimental results. *Ann. Nucl. Energy* **53**, 529–534 (2013). doi:[10.1016/j.anucene.2012.09.015](https://doi.org/10.1016/j.anucene.2012.09.015)
- J.K. Shultis, R.E. Faw, *An MCNP primer* (Department of Mechanical and Nuclear Engineering, Kansas State University, Manhattan, 2010)
- J.H. Hubbell, S.M. Seltzer, *Tables of X-ray mass attenuation coefficients and mass energy-absorption coefficients 1 keV to 20 MeV for elements Z = 1–92 and 48 additional substances of dosimetric interest*, NISTIR 5632. National Institute of Standards and Technology, Gaithersburg (1995)
- L. Gerward, N. Guilbert, K.B. Jensen et al., X-ray absorption in matter. Reengineering XCOM. *Radiat. Phys. Chem.* **60**, 23–24 (2001). doi:[10.1016/S0969-806X\(00\)00324-8](https://doi.org/10.1016/S0969-806X(00)00324-8)
- L. Gerward, N. Guilbert, K.B. Jensen et al., WinXCom: a program for calculating X ray attenuation coefficients. *Radiat. Phys. Chem.* **71**, 653–654 (2004). doi:[10.1016/j.radphyschem.2004.04.040](https://doi.org/10.1016/j.radphyschem.2004.04.040)
- F. Demir, G. Budak, R. Sahin et al., Determination of radiation attenuation coefficients of heavyweight- and normal-weight concretes containing colemanite and barite for 0.663 MeV γ -rays. *Ann. Nucl. Energy* **38**, 1274–1278 (2011). doi:[10.1016/j.anucene.2011.02.009](https://doi.org/10.1016/j.anucene.2011.02.009)
- G.F. Knoll, *Radiation Detection and Measurement*, 3rd edn. (Wiley, New York, 2000)
- A. Un, Y. Sahin, Determination of mass attenuation coefficients, effective atomic and electron numbers, mean free paths and kermas for PbO, barite and some boron ore. *Nucl. Instrum. Methods B* **269**, 1506–1511 (2011). doi:[10.1016/j.nimb.2011.04.011](https://doi.org/10.1016/j.nimb.2011.04.011)
- N. Singh, K.J. Singh, K. Singh et al., Comparative study of lead borate and bismuth lead borate glass systems as gamma-radiation shielding materials. *Nucl. Instrum. Methods B* **225**, 305–309 (2005). doi:[10.1016/j.nimb.2004.05.016](https://doi.org/10.1016/j.nimb.2004.05.016)